Green Chemistry

Accepted Manuscript

This is an *Accepted Manuscript*, which has been through the Royal Society of Chemistry peer review process and has been accepted for publication.

Accepted Manuscripts are published online shortly after acceptance, before technical editing, formatting and proof reading. Using this free service, authors can make their results available to the community, in citable form, before we publish the edited article. We will replace this *Accepted Manuscript* with the edited and formatted *Advance Article* as soon as it is available.

You can find more information about *Accepted Manuscripts* in the Information for Authors.

Vapor phase hydrodeoxygenation of anisole over ruthenium and nickel supported mesoporous aluminosilicate

Sudhakar Pichaikaran, Pandurangan Arumugam[*]

Department of Chemistry, Anna University, Chennai 600 025, India

*Corresponding author at: Tel.: +91 44 22358653; fax: +91 44 22200660.

E-mail address: pandurangan_a@yahoo.com (A. Pandurangan)

Graphical abstract,
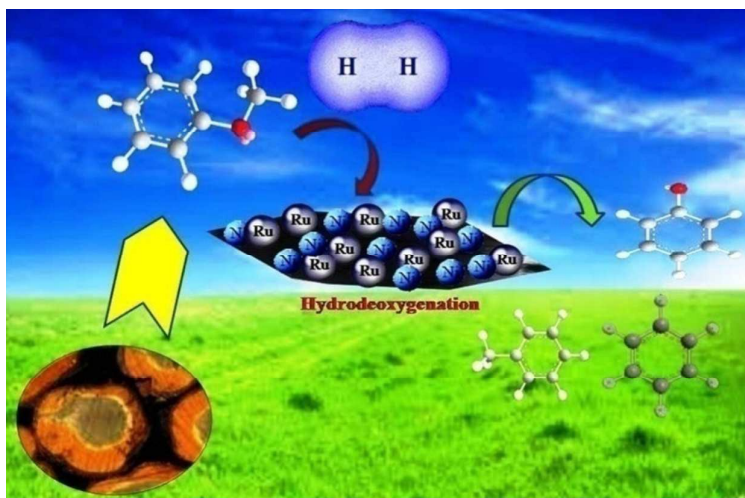
Abstract

Mesoporous aluminosilicate (Al-SBA-15) support synthesised via direct hydrothermal method was post loaded with mono-metals such as 1.0 wt% RuO_2 and 7.0 wt% NiO separately. Furthermore, different weight percentage of bimetallic catalysts such as RuO_2 (0.2-1.0 wt %) with 7.0 wt% NiO were loaded jointly on mesoporous Al-SBA-15 support by wet impregnation method for hydrodeoxygenation of anisole. The XRD and BET results revealed that the materials were hexagonally ordered indicating the presence of mesoporosity. NH_3-TPD results confirmed the presence of acidic sites on materials, which enhanced HDO activity of anisole. The oxidation state of Ni^{2+} and Ru^{4+} was confirmed by XPS analysis. H_2 - TPR revealed the strong metal-support interaction in mono-metal catalyst of 7.0 wt% NiO whereas, in the case of bimetallic catalysts the reduction temperature of Ni was lowered below 440 ^{o}C by the addition of Ru which is lower than the that of 7.0 wt% NiO (524 ^{o}C). The HR-TEM images further confirmed the presence of mesoporous nature along with RuO_2 and NiO crystallites largely located over the surface of Al-SBA-15. The activity of all the

synthesised catalysts was tested over vapour phase hydrodeoxygenation of anisole (bio-mass compound).Variation of temperature and time on stream with atmospheric pressure was optimised to obtain high conversion and selectivity. Reaction temperature of 400 ^{o}C was found to be optimum. The 1.0 wt% RuO_2/7.0 wt% NiO catalyst gave highest conversion about 46% of anisole and selectivity towards benzene of 45%. Bimetallic catalysts (1.0 wt% RuO_2/7.0 wt% NiO) showed high activity compared to mono-metallic catalysts (1.0 wt% RuO_2 and 7.0 wt% NiO) due to the synergism of Ni and Ru. Also the bimetallic catalysts showed good activity compared to other reported catalysts under variable experimental conditions.

Keywords: Anisole, Hydrodeoxygenation, Benzene, RuO_2-NiO/Al-SBA-15, RuO_2/Al-SBA-15, NiO/Al-SBA-15.

1 .Introduction

Lignocellulosic biomass is one of the important sources of renewable feedstock for fuels and chemicals. In recent days, is being a challenge to reduce our dependence on petroleum and natural gas. Further an increasing attention has been focused in alternative liquid fuel because of the depletion of petroleum deposits and also the increasing environmental concern. Fast-pyrolysis of lignocellulosic biomass leads to a liquid bio-oil which contains more concentration of small oxygenates. Hence, it could not be directly used as fuel due to difficult operational conditions including low pH, low heating value, high viscosity, thermal and chemical instability and immiscibility with hydrocarbon fuels. Therefore, building up the carbon chain is an important milestone for small oxygenates conversion for obtaining sustainable fuels from lignocelluloses biomass[1]. Anisole is one of the major species identified in bio feeds of lignocellulosic origin. The origin of these compounds may be deduced from the model structure of lignin, an important constituent lignocellulosic biomass [2]. Anisole contains an isolated methoxyl, one of the major functional group of the lignin phenolic and is liquid at room temperature and hence no solvent is needed in both reaction and analysis[3]. Compared to other thermochemical process hydrodeoxygenation is one of the potential techniques to transform lignocellulosic biomass into commodity fuels and chemicals[4]. The complete hydrodeoxygenation and hydrogenation of aromatics and other oxygenated compound over metal sites is predetermined to give hydrocarbons under high pressure but the demand of hydrogen consumption is high in this process. Hence, minimizing hydrogen consumption and carbon losses are important key aspects to reducing the cost of biomass

derived liquid fuel. Moreover, production of benzene and toluene from lignin fraction is an economically favourable process in petrochemical industry for replacing fossil feedstock to renewable resources [5].

Traditional hydrodeoxygenation process based on Co-Mo and Ni-Mo sulphated catalyst can effectively reduce oxygen content in phenolic bio-oil[6], even though these types of catalyst produce high sulphur stream it create significant loss of active sites in the catalyst as a result of liquid yield decreased[7]. Currently the challenge is to design new bifunctional (acid and metal) catalysts are needed for hydrgenolysis and hydrogenation of the carbon-oxygen bond of anisole and capable of maintaining stability during the time on stream condition of anisole hydrotreatment[8]. Supports could play a vital role in dispersing active metal component, stabilize the small metallic particles and enhancing the metal support interaction and further the catalytic activity. The influence of supports like TiO_2, Al_2O_3, ZrO_2 and SiO_2 is well recognized but the development of new support is of great interest in catalysis[9,10]. In these aspects, the discovered mesoporous SBA-15 aluminosilicate employ as the catalyst support possessing high surface area, uniform hexagonal channels, thicker pore walls, larger pore size and considerable hydrothermal stability might be a good candidate to design the bifunctional catalyst used in the conversion of anisole[11] . In the present study, 7.0 wt% Ni/Al-SBA-15, 1.0 wt% Ru/Al-SBA-15 and (0.2, 0.4, 0.6, 0.8, 1.0 wt% Ru)/7.0 wt% Ni/Al-SBA-15 mono and bimetallic catalysts was prepared using wet impregnation method and investigated their catalytic efficiency over hydrodeoxygenation of anisole under different temperatures and atmospheric pressure condition. The crystalline phase identification of active metal, morphology of the support, textural properties and surface metal- acid function was studied. Based on these studies the correlations between the catalytic activity and surface metal acid functions were further investigated.

2. Experimental

2.1. Materials

Tetraethylorthosilicate (TEOS; Aldrich) used as silica source, Triblockcopolymer (Pluronic P123, EO_{20} PO_{70} EO_{20}; Aldrich: M.W.5800) were used as AR grade chemicals (>98 % pure). Hydrochloric acid (35 %) used in the synthesis were AR grade chemical. Anisole was purchased from SRL Biochem (India) Ltd. (99 % pure). Aluminium isopropoxide (Alfa-Aesar), Nickel (II) nitrate hexahydrate (Aldrich) and Ruthenium trichloride trihydrate (SRL

Biochem India Ltd) were used as active metal sources and all chemicals were used without further purification.

2.2. Synthesis of Catalysts

Al-SBA-15 with Si/Al ratio 25 was synthesised by according to reported literatures [12]. Typically, Pluronic (P123)   4 g was added to 30 mL of deionised water in a polypropylene bottle after stirring for 4 h, a clear solution was obtained. About 70 g of 0.28 M hydrochloric acid was added and stirring was continued for another 2 h. Then 9 g of TEOS and calculated amount of Aluminiumisopropoxide were added and the resulting mixture was stirred at 40 °C for 24 h and placed in an oven at100 °C for 48 h. The resulting solid material was recovered by filtration, washed with several times with distilled water and dried overnight at 100 °C, finally the material was calcined at 540 °C for 6 h in order to remove the template. 1.0 wt% RuO_2/Al-SBA-15, 7.0 wt% NiO/Al-SBA-15 and (0.2, 0.4, 0.6, 0.8, 1.0 wt% RuO_2)/7.0 wt% NiO/Al-SBA-15 was prepared by wet impregnation method. 1.0g of synthesised Al-SBA-15 was transferred to 50mL round bottom flask added 25 mL of deionised water stirred for 15 minutes a homogeneous mixture was obtained and required wt% of metal sources was dissolved in 10 mL of deionised water and added drop by drop in to the mixture. After stirring for 6 h water was removed by evaporation and drying at 100 °C for 12 h and calcined in atmospheric air at 400 °C for 6 h.

2.3 Characterization of support and catalysts

X-ray diffraction (XRD) pattern of metal impregnated calcined materials was obtained using (PAN Analytical, diffractometer) using nickel filter Cu Kα radiation (λ=1.5406 Å). The crystalline phase was identified by matching the peaks with appearing in the XRD pattern of the test sample with JCPDS (joint committee on powder diffraction standards) data files. Surface area was calculated by the BET method (Quanta chrome 2010-09). The N_2 adsorption desorption isotherm was obtained at liquid nitrogen temperature. Pore volume and average pore size were calculated by BJH method. Metal content was determined by ICP-OES Perkin Elmer Optima 5300Dv instrument. H_2- TPR characteristics of the oxide catalysts were obtained using (Quanta chrome 2010). About 100 mg of the dried sample was used for each measurement the sample was pre-treated at 115 °C in high pure Helium gas (25 cc/min) for one hour and cooled to room temperature and then, the gas was changed to mixture of 5vol % H_2/Ar (25 cc/min) introduced in to the sample tube at room temperature till baseline is stable. Then TPR started from room temperature to 800 °C at 10 °C/min. NH_3-TPD were

carried out in a flow reactor (micrometrics instrument corporation chemisoft TP ×V1.02 unit 1-2750). Samples were activated at 500 °C for 1 h in a flow of Helium in addition to 10 vol.% NH_3 was introduce by a steam of Helium at 100 °C. The physically adsorbed NH_3 was removed by purging with a Helium flow at 100 °C until the base line was flat. Then the desorption temperature was started from 100 °C to 500 °C at a rate of 10 °C/min. XPS was performed in a Omicron Nanotechnology, GmBH, Germany XM1000 monochromated with Al K_α radiation of 1,483eV operated at 300 W (20 mA emission current, 15 kV) and a base pressure in the analysis chamber was better than 5×10^{-5} mbar. The survey spectrum was performed with a step size of 0.5 eV along with 50 eV as the pass energy. HR-TEM images were obtained on a TECNAI T30 G^2 FEI company and an accelerating voltage of 300 kV. The samples for the HR-TEM study were prepared by ultrasonic dispersing in acetone for one hour and consequent deposition of the suspension on a Copper grid and dried 37 °C for 30 min and examined under HR-TEM.

2.4 Catalytic experiment

Hydrodeoxygenation of anisole was studied in a fixed- bed, down flow reactor made up of quarts tube of length 40 cm and internal diameter 2 cm, using 7.0 wt% Ni/Al-SBA-15, 1.0 wt% Ru/Al-SBA-15 and (0.2, 0.4, 0.6, 0.8, 1.0 wt% Ru)/7.0 wt% Ni/Al-SBA-15 catalysts. The reactant flow was fed into the reactor using syringe infusion pump (Ravel Hiteks, India). About 0.3 g of catalyst placed in the reactor tube and supported on either side with thin layer of quarts wool and ceramic beds. The reactor was heated to reaction temperature with the help of a tubular furnace controlled by a digital temperature controller. The bottom of the reactor tube was connected to a coiled condenser and a receiver to collect the product, before starting of the reaction, the oxide catalyst was reduced in the presence of Hydrogen 50 mL/min at 500 °C. The reaction was carried out at atmospheric pressure and reaction temperature over 300 °C to 450 °C, WHSV 4.1771 h^{-1}; H_2=50 mL/min, Anisole flow rate 1 mL/h. The liquid product collected during 10 min was discarded and the product collected after every hour interval was analysed by off-line gas chromatograph (GC-17A Shimadzu) using a FID detector and Rtx-5 (30.0 m×0.25 mm, 0.25 um film thickness) column.

3. Results and discussion

3.1. Physicochemical characteristics of the support and catalysts

3.1.1. XRD studies

The low and high angle X-ray diffraction patterns of all the calcined catalysts are shown in Fig.1 (a) and (b). The physico-chemical properties of various metal impregnated over mesoporous SBA-15 catalysts are presented in Table 1.The low angle XRD pattern of Al-SBA-15 showed three well resolved peaks at $2\theta=0.90^{o}$,1.55^{o} and 1.77^{o} is characteristics of (100), (110) and (200) reflections of hexagonal lattice (p6mm) space group symmetry, indicating ordered mesostructure. The unit cell parameter a_o value calculated from the $d_{(h\ k\ l)}$ (100) spacing in the XRD pattern is 15.7 nm, which confirmed the formation of mesoporosity and crystalline nature of Al-SBA-15[12]. While, ruthenium and nickel supported oxide materials shows slight peak shifted at $2\theta=0.99^{o}$, 1.63° and1.84° and corresponding to unit cell parameter a_o value for d $_{(h\ k\ l)}$ 100 spacing is 10.2 nm. The peak intensity and a_o value of oxide catalyst slightly decreased this could be due to the presence of small amount of metal oxide particle which occupied on the pores of the materials. However it does not significantly change the hexagonal ordering of Al-SBA-15 framework as seen from the N_2 sorption isotherms Fig. (2), and also confirmed from HR-TEM images Fig. (6). In the case of wide angle XRD pattern of all the material showed the broad diffraction peak around 22° attributable to amorphous silica, as it is usually found for these mesoporous material, which consist of an ordered array of channels in a non- crystalline matrix of SiO_2 and a strong peak at $2\theta= 37.2^{o}$, 43.2^{o} and 62.8^{o} corresponding to (111), (200), (220) plane of cubic NiO[13,14] . The pattern reveals that ruthenium metal oxide on the parent material of Al-SBA-15 show distinct crystalline phase corresponding to reflections at (110), (101), (210), (211) and (311) of tetragonal RuO_2 phase [(JCPDS Card No: 65-2824)]. These patterns suggest that the intensity of RuO_2 phase gradually decreases as the ruthenium weight percentage from 1.0 to 0.2. Crystallite sizes of NiO phase and RuO_2 phase, calculated from the line broadening of (200) and (210) diffraction using the Debey-Scherrer equation, are listed in the Table. 1. The crystallite size of mono metallic catalyst shows small but in the case of bimetallic catalyst some extent bigger, even though the particle was uniformly dispersed over the surface of the support; this was identified from the HR-TEM images.

3.1.2. N_2 Sorption analysis

Nitrogen adsorption-desorption isotherms and pore size distribution of all the catalyst are shown in Fig. 2 (a) and (b). The BET surface area, pore volume and average pore size of entire catalyst are listed in Table 1. All the obtained isotherms are of irreversible type IV according to IUPAC classification and exhibited an H1 broad hysteresis loops. Such type of loops can be referred to the presence of uniform cylindrical pores of relatively large

dimensions [12]. The impregnation of metal oxides in Al-SBA-15 could not affect the shape of adsorption isotherm on pure support these was confirmed by BJH isotherm and low angle XRD. Al-SBA-15 showed high surface area with large pore volume confirming the expansion of the mesopores upon introducing Al into the SBA-15 framework. Impregnation of NiO and RuO_2 in different wt. % into Al-SBA-15 lead to a gradual decrease in surface area, pore volume and pore wall thickness this is due to utilization of surface hydroxyl group of support by reaction with active metal oxide phase. Such a surface reaction might have caused the decrease of available surface area of the support, possibly by closure of the pores as evidenced by pore size distribution[11].

3.1.3. NH_3- TPD Analysis

The NH_3-TPD spectra of oxide catalyst are shown in Fig. 3. The total acidity values obtained from the TPD profiles for oxide catalyst are listed in Table 1. The total acidity of the catalyst is given by area under the TPD curve. The acid site distribution of all the catalysts was obtained from the amount of ammonia desorbed at different temperatures. Generally, the acid sites are classified in to weak (<200 °C), medium (200 °C – 300 °C) and strong (>350 °C) acid sites[15]. The incorporation of Al in the frame work of SBA-15 was generating both Bronsted and Lewis acid sites. The desorption of ammonia over Al-SBA-15 shows shoulder peak in the range at 127 °C to 227 °C is attributed to weak and medium acid sites. The total peak area under the ammonia desorption for Al-SBA-15 is larger than that of metal oxide containing materials, mostly abundant with weak acid sites. 1.0 wt% RuO_2/Al-SBA-15 showed weak and medium acid sites at 178 $^{\circ}$C and 266 $^{\circ}$C with respect to NH_3 desorption. At the same time, 7.0 wt% NiO/Al-SBA-15 showed weak and strong acid sites corresponding to NH_3 desorption occurred at 174 $^{\circ}$C and 349 °C. All the bimetallic catalyst mostly gives weak and strong acid sites and the large amount of desorption of NH_3 was observed at >350 $^{\circ}$C as maxima reveals that the strong acidity is generated on the surface of all the bimetallic materials. The acidity of bimetallic catalyst gradually increases in RuO_2 loading up to 1.0 wt%. However total acid sites in the case of bimetallic catalyst found to be higher than mono metallic catalyst. The results indicated that the catalytic activity increase with respect to increasing acidity values. The hydrgenolysis of anisole needs medium to strong acid sites to produce benzene, and the selectivity of benzene is proportional to acidity of the catalysts.

3.1.4. XPS Studies

Oxidation state and chemical composition of ruthenium and nickel supported Al-SBA-15 catalyst are given in Fig 4 with insets. The +4 oxidation state of Ru was identified from Ru 3d doublet (5/2 and 3/2) with binding energy value of 280.5 eV and 284.5 eV and corresponding oxygen 1s peak appeared at 535.4 eV[16]. The Si2p core level spectrum was identified at binding energy value of 103.2 eV which is characteristics of Si^{4+} species in silicate frame work of support[8]. The XPS pattern revealed that there is two spin states were identified for Ni2p spectra, which is $Ni2p_{1/2}$ and $Ni2p_{3/2}$. The spin state corresponding to binding energy value of 874.4eV and 856.5 eV is assigned to nickel in +2 oxidation states. In contrast to $Ni2p_{3/2}$, peak shifted towards higher binding energy value around 2.1 eV compared to that of pure NiO (854.4 eV) as value obtained from other literature results. This factor suggests that the addition of Ru was enhancing higher binding energy value of nickel. Further, it confirmed that higher proportion of NiO specie form than the other forms and the blue shift in the $2p_{3/2}$ peak can be assigned to existence of small nickel oxide particle inside the pores of support due to higher loading of nickel oxide than ruthenium oxide and this can be agree with N_2 sorption analysis. In general, the XPS patterns revealed that ruthenium and nickel crystallites were well dispersed in to pore wall of surfaces over support was confirmed from other reported results [17].

3.1.5. H$_2$-TPR Analysis

Fig. 5 represents the H_2-TPR profiles of mono and bimetallic of Ni and Ru (oxides) supported Al-SBA-15 catalysts. All the supported metal oxide catalysts were completely reduced below 530 ^{o}C. The reduction behaviour of monometallic ruthenium oxide catalyst was observed at 164 ^{o}C this reduction temperature indicate, RuO_2 more easily reduced to Ru and this denoting weak metal-support interaction. In contrast to monometallic nickel oxide catalyst, contribute two distinct shoulder peaks around 375 ^{o}C and 524 ^{o}C. The peak at 375 ^{o}C indicates the high amount of Hydrogen was desorbed over the surface nickel oxide species and sharp reduction peak around 524 ^{o}C indicate nearly lower amount of Hydrogen was desorbed. These results suggest that the former desorption temperature indicate the presence of more exposed surface nickel oxide species and is assigned to transition of NiO into Ni and the higher desorption temperature generate stronger metal support interaction which is created by presence of acidic sites in the support[18]. However, in the case of bimetallic catalyst, the nickel oxide peak shifted towards lower reduction temperature 310 ^{o}C, this suggest that the addition of ruthenium metal site should enhance splitting of more molecular hydrogen in to atomic

hydrogen, i.e., Ni^{2+} cations more rapidly reduced by atomic hydrogen than molecular hydrogen[19]. The reduction temperatures of bimetallic Ni^{2+} species has considerably lower than monometallic Ni^{2+} species[20]. A lower temperature shift of almost 100 ^{o}C was observed.

3.1.6. HR-TEM Analysis

The morphology and metal size distribution of 1.0 wt% RuO_2/7.0 wt% NiO/Al-SBA-15, 7.0 wt% NiO/Al-SBA-15 and 1.0 wt% RuO_2/Al-SBA-15 are shown in Fig. 6. Mesostructured nature with regular array of pores further confirmed morphology of Al-SBA-15 and was retained even after high loading of active metal over the support. Fig. 6(a) indicates that NiO/RuO_2 particles are shown as black dots on the surface of the support material and exist as well dispersed state. The average particle size distribution of RuO_2/ NiO was found relatively ranging from 20-110 nm, however the maximum particle size distribution of about 60 nm was observed as comparable with crystal size calculated from Debye-Scherrer equation obtained from high angle XRD results (Table.1). Mono-metallic catalysts considerably show the small particle size than bimetallic catalysts are presented in the Fig. 6(b), (c). Hence, the interaction between NiO and RuO_2 with support much weaker compared to mono metallic catalyst as a result agglomeration take place this factor which favours to increasing bigger particle size in bimetallic catalyst [21]. Since, the majority of particles most likely present over surface of the support, this was further supported by XPS studies.

3.2. Catalytic process of Anisole

The catalytic process of anisole was investigated under operating condition (T=300 ^{o}C to 450 ^{o}C, atmosphere pressure, H_2=50mL/min, flow rate of anisole 1mL/h, WHSV=4.1771 h^{-1}). The most significant products obtained by hydrodeoxygenation of anisole are benzene, phenol and trace amount of toluene. Anisole conversion was obtained at different temperature over all the catalysts are presented in Fig. 7a-g. The conversion related to temperature with time on stream study was investigated under this set of experimental condition, the maximum conversion was observed at 400 $^{\circ}$C for all the bimetallic catalyst except 0.2 wt% Ru/7.0 wt% Ni and mono metallic catalyst. The mono metallic catalyst showed maximum conversion at 450 $^{\circ}$C and below these temperature shows lower conversion and this indicate that the catalyst become activation energy is demanding and it revealed that a reaction temperature 300 $^{\circ}$C to 350 $^{\circ}$C may not be sufficient to activate reacting molecule to obtain better conversion. At lower temperature mono oxygenated intermediate of phenol was

predominately measured and the selective product towards benzene and toluene was not observed highly. This suggest that phenol intermediate is adsorbed on the active catalytic surface, which are not further changes to secondary deoxygenated product at lower temperature. Mostly the conversion was suppressed after phenol intermediate formation at lower temperature. In the case of 0.2 % Ru/7.0 Ni/AlSBA-15 shows maximum conversion at 300 °C and 350 °C is 3.0 % and 5.8 %. The conversion with respect to low temperature at 300 °C for 1.0 % Ru/7.0 % Ni/AlSBA-15 and 0.8 % Ru/7.0 % Ni/AlSBA-15 shows less than 2.0 % and at 350 °C shows 15.0 % and 7.0 % respectively. Where as in the case of 0.4 % Ru/7.0 % Ni/AlSBA-15 and 0.6 % Ru/7.0 Ni/AlSBA-15 shows maximum conversion at 300 °C is 4.3 % ,5.6 % and for 350 °C 8.5 % and 8.2 %. Thus the high temperature is needed to activate intermediate phenol molecule to secondary deoxygenated product of benzene. This suggests that increasing the temperature could promote high conversion. With respect to time on stream at 450 °C for 0.2 wt% Ru loading catalyst shows that the conversion increases initially and beyond 15h the conversion decreased, at that maximum point the deoxygenated product benzene was observed at 26 %. So, the same trend was observed at 400 °C for rest of the bimetallic catalyst. Among the bimetallic catalyst 1.0wt%Ru/7.0wt%Ni initially gives maximum conversion 46.0 %, this may be due to uniform distribution of the active particles through the mesopore of the support as observed from TEM images Fig 6 (a) and the good accessibility of the reactants to ruthenium and nickel phase deposited on the mesopore may increases the catalytic conversion. The dependence of HDO activity on the surface acidity of the catalyst as measured by desorbed NH_3 in TPD, was also considered but the surface acidity of all catalyst are not highly different. Though, 1.0 % Ru/7.0 % Ni/AlSBA-15(25) had higher acidity value (Table 1) this may favour the hydrogenolysis reaction path way in the catalytic route. With respect to product selectivity, oxygen free product significantly decreases at lower time on streams but increases with higher time on streams. In the case of Ni and Ru supported mono metallic catalyst, anisole conversion were 19.8 % and 7.6 % respectively. Significantly, the product distribution is entirely different compared to that bimetallic catalyst. Particularly, 1.0wt%Ru monometallic catalyst gives only phenol and benzene and these results denote that demethylation followed hydrgenolysis route is the main pathway (Fig.9) of this catalyst. In contrast, product distribution obtained over 7.0 wt% Ni shows phenol, benzene and toluene. This product distribution corresponds with hydrgenolysis/methyl transfer route. Therefore, the same reaction trend was obtained for all the bimetallic catalysts.

The product selectivity of all the catalyst with respect to time on stream was investigated Fig. 8a-g. Under this present experimental condition, the significant difference observed in product distribution may be due to the strong influence of acidic support and, their bimetallic system. The major product benzene and phenol followed by trace amount of toluene was observed for all the bimetallic catalyst. It is also noted that 1.0 wt% Ru mono metallic catalyst obtained major products as benzene and phenol. The deoxygenated product of benzene for bimetallic catalysts gives maximum of 61.6 % for the case of 0.4 wt% Ru. While other weight percentage of catalyst (% Ru) given by the following order 1.0 (45.4 %)>0.6 (44.5 %)>0.2 (36.1 %)>0.8 (34 %). Where as in the case of mono metallic catalysts, the deoxygenated product of benzene were found to be 38 %, 34.9 % for 1.0 wt% Ru and 7.0 wt% Ni respectively.

A large synergy effect between nickel and ruthenium was observed for the HDO reaction. The Allred Rochow electronegativity for nickel atom is 1.75 and ruthenium atom is 1.42, nickel oxide draws electron more strongly from ruthenium oxide, this factor may influence existence of larger surface nickel atom than bulk nickel atom. So this surface nickel can split more molecular hydrogen in to atomic hydrogen and this may utilized for the formation of benzene in HDO reaction. The random dispersion of the active metallic sites and existence of variable metal particle sizes in the bi-metallic catalysts would have altered the benzene selectivity. Usually, uniform dispersion of particle size can effectively catalyse the reaction and this type of behaviour was considerably observed only with 1.0 % Ru/ 7.0 % Ni/AlSBA-15 catalyst as seen in TEM images Fig. 6(a).

The comparisons with respect to references 5, 21-24 with their experimental conditions are employed and compared with the present catalysts under consideration. Many of the studies have been carried out at higher pressure, while our study with metal supported acidic catalysts has been done at atmospheric pressure condition. However, HY Zeolite was also carried out at atmospheric pressure which resulted with negligible amount of HDO product. This reveals that the addition of ruthenium over nickel based acidic mesoporous catalyst with synergism showed comparable effective results with other type of catalysts under our experimental condition as shown in Table. 2. The time-on-stream behaviour of catalyst showed that the conversion is stable up to 15 h on stream and beyond this limit the conversion gradually decreased due to loss of active sites on catalyst by the formation of coke. Thermogravimetric analysis of the spent catalyst was carried out to estimate the coke deposit after reaction with anisole as shown in Fig (10). The thermogram shows the following

increasing order for the formation of coke in the bimetallic catalyst 3.5%<4.8 %<5.0 %<5.2%<6.8% for 1.0 % RuO /7.0 NiO, 0.8 % RuO_2 /7.0 NiO , 0.6 % RuO_2 /7.0 NiO , 0.4 % RuO_2 /7.0 NiO and 0.2 % RuO_2 /7.0 NiO respectively. With respect to mono metallic catalyst, 7.0 % NiO gave 8.0 % weight loss and 1.0 % RuO_2 gave 8.7 % weight loss. In general, the formation of coke on the mono metallic catalyst was higher than bimetallic catalyst. The major weight losses have been observed at 330 $^{\circ}$C. These results indicate that the catalytic performance in terms of conversion was suppressed by formation of coke and this factor was minimized by increasing ruthenium Wt. %. The sintering of active species during HDO reaction was not identified as confirmed from existence of active crystalline phase in the catalysts after reaction with anisole as shown in Fig. 11. Sinter resistant at high temperature may be due to presence of strong metal support interaction in the catalyst as further supported by reductive environment in the H_2 TPR analysis Fig 5. The loss of activity was mainly caused by coke formation but not sintering.

The product formation over anisole conversion was reported by many workers[22–25]. In the present study, phenol, benzene and toluene were identified as major products and also benzene is one of the most abundant products in all the catalysts. Fig. 9 is a plausible reaction scheme representing anisole conversion. Pathway (a) is demethylation, which takes place on the metal surface. Another reaction pathway (b) involves methyl group transfer which is also takes place over metal site. On catalyst that contains both metal and acid sites, in addition to pathway (a) and (b) hydrgenolysis of phenol and methyl phenol catalysed by acid sites via pathway (c).This indicates that the presence of both metal and acid site on catalyst favours oxygen removal [22,26]. The direct deoxygenating route product of methanol was not observed over all the catalyst , suggesting that catalyst are very much selective in nature in cleaving C-O bonds instead of phenolic C-O bonds of anisole[27]. Also, the ratio of product distribution (benzene: toluene) was calculated with respect to all the bimetallic catalyst and generally it follows the trend as (17:1), except 0.2 % RuO_2 /7.0 NiO (14:1).

The reaction proceeds in two path ways i) HDO route and ii) trans-methylation. The HDO path requires two types of active sites one is activation of dihydrogen and another one is desirable metal site for activation of oxy-group. Thus, the two main routes of anisole transformation can be driven by adsorption configuration of substrate molecule i.e., the adsorption through the oxygen bond may favour demethylation where as π-bond adsorption leads to the hydrogenation of the aromatic ring. Therefore, the surface characteristics of the catalysts explain the variation in product selectivity[22,26,28]. The surface of the catalyst is

influenced by adsorption through oxygen bond may favour HDO route. On the basis of (Figs. 7, 8) data showing that phenol was identified as the primary intermediate so that demethylation was identified as most frequent class of reaction, during the demethylation of anisole the presence of Lewis acid sites on the catalyst could accept free lone pair electron from oxygen atom of anisole forming a weak coordinative bond, followed by the heterolytic scission of the $C_{methyl} - O$ bond, after formation of phenol is converted to benzene via the direct hydrogenolysis of $C_{aromatic}$-O bond. Methyl group transfer (transalkylation) are the another path of reaction. In this catalytic path, methyl phenol has the intermediate and this intermediate was not identified may be due to the formation of this intermediate very short life time in the catalytic path but slightly lesser amount of toluene was obtained from hydrgenolysis of methyl phenol intermediate. So, the catalytic path was suggested that, the catalyst predominately work through demethylation. The phenol formation reaction was take place on metal site by cleavage of O-CH$_3$ which enhances the overall formation of benzene. On the other hand, methyl group that are produced on active metal site are transfer to other aromatics and this transformation not only take place by metal site, as well as metal site contact with acid sites which generate synergistic effect and this effect not pronounced effectively for methyl transfer reaction because we observed only lesser amount of toluene formation from the methyl phenol intermediate. Therefore, demethylation reaction path was more frequent than methyl transfer reaction.

In the case of bimetallic catalyst high HDO product selectivity was obtained than mono metallic catalyst and the presence of medium acid sites may contribute small extent of trans-methylated product of toluene. Among the bimetallic catalysts 0.4 wt% Ru/7.0 wt% Ni showed higher amount of product selectivity towards benzene. The direct hydrogenated product of methoxycyclohexane and aromatic ring hydrogenated product of cyclohexane was not found for all the catalysts. These results indicate that catalyst become completely inactive for hydrogenation of aromatic ring; this may be the presence of oxygen containing species from reactant, which prevent hydrogenation activity of catalyst[29].We propose that the addition of ruthenium into nickel has enhanced the high dispersion of catalyst, which could lead to higher metallic sites and also the presence of aluminium in the support generate more acidic centres in the catalyst which contribute high degree of HDO products selectivity than methylated product.

4. Conclusions

The performance of mono versus bimetallic catalytic system with nickel and ruthenium supported Al-SBA-15 obtaining broad range of physicochemical properties was investigated and tested for the hydrodeoxygenation of anisole. The wide angle XRD and XPS analysis revealed the formation of cubic NiO and tetragonal RuO_2 phase on support. The N_2 sorption analysis showed that surface area and pore diameter of the materials diminished with metal wt% increases due to penetration of metal oxides into the pores. Based on temperature and time on stream studies, 1.0 wt% Ru/7.0 wt% Ni over mesoporous aluminosilicate was found to be superior in catalytic activity and selectivity towards benzene production, which is due to the presence of acidic sites and bimetallic particles. The presence of acidic sites contributes the hydrogenolysis of anisole to produce benzene and further hydrogenation at metal site was restricted. The addition of Ru reduces the reduction temperature of Ni and generates weak interaction between Ni and support on bimetallic catalysts lead to high anisole conversion and selectivity. Among bimetallic catalysts 0.4 wt% Ru/7.0 wt% showed highest selectivity towards benzene formation. The product formation over all the catalysts proves a plausible reaction sequence including hydrodeoxygenation, hydrogenolysis and methyl transfer. The significant improvement in catalytic activity is well dispersion of Ru and Ni particles on Al-SBA-15 matrix and also the presence of acidic sites. Therefore, it can be concluded that a suitable selection of bimetallic catalysts show excellent catalytic performance for production of deoxygenated aromatics from biomass derived lignin feedstock.

Acknowledgements

Table Captions:

Table. 1. Textural Properties, surface acidity and crystallite size of metal on supported catalysts

Table. 2. Comparison between HDO results from literature.

Figure Captions:

Fig. 1. XRD patterns of calcined support and metal oxide supported materials (a) low angle and (b) high angle.

Fig. 2. (a) Nitrogen adsorption desorption isotherms at 77K (b) pore size distribution applying BJH method in the adsorption branch.

Fig. 3. Ammonia-TPD profiles for metal oxide catalysts supported on Al-SBA-15

Fig.4. XPS spectrum of (a) 1.0 wt% RuO_2/7.0 wt% NiO/Al-SBA-15, (b) 0.2 wt% RuO_2/7.0 wt% NiO/Al-SBA-15 and inset Ru3d, Ni2p

Fig. 5. TPR profiles for various metal oxide supported on Al-SBA-15 catalysts

Fig.6. HR-TEM images and metal size distribution of oxide catalyst (a) 1.0 wt% RuO_2/7.0 wt% NiO/Al-SBA-15 (b) 7.0 wt% NiO/Al-SBA-15, (c) 1.0 wt% RuO_2/Al-SBA-15

Fig.7. Effect of temperature on anisole conversion with respect to time-on-stream a) 1.0 wt% Ru/Al-SBA-15 , b) 7.0 wt% Ni/Al-SBA-15 , c) 0.2 wt% Ru/7.0 wt% Ni/Al-SBA-15 , d) 0.4 wt% Ru/7.0 wt% Ni/Al-SBA-15, e) 0.6 wt% Ru/7.0 wt% Ni/Al-SBA-15 , f) 0.8 wt% Ru/7.0 wt% Ni/Al-SBA-15 , g) 1.0 wt% Ru/7.0 wt% Ni/Al-SBA-15.Conditions: WHSV (h^{-1}) =4.1771; atmosphere pressure; H_2=50mL/min, Anisole flow rate =1.0 mL/h

Fig. 8. Evaluation with the time-on-stream of the anisole selectivity to phenol, benzene and toluene for a) 1.0 wt% Ru/Al-SBA-15 , b) 7.0 wt% Ni/Al-SBA-15 , c) 0.2 wt% Ru/7.0 wt% Ni/Al-SBA-15 , d) 0.4 wt% Ru/7.0 wt% Ni/Al-SBA-15 , e) 0.6 wt% Ru/7.0 wt% Ni/Al-SBA-15, f) 0.8 wt% Ru/7.0 wt% Ni/Al-SBA-15 , g) 1.0 wt% Ru/7.0 wt% Ni/Al-SBA-15. Conditions: WHSV (h^{-1}) =4.1771; atmosphere pressure; temperature=400-450 $^\circ$C; H_2=50mL/min, Anisole flow rate =1.0 mL/h

Fig. 9. Scheme of the possible routes for anisole hydrotreating

Fig. 10. Thermal gravimetric analysis of coke catalyst

Fig. 11. XRD pattern of spent catalyst

Table 1.

Sample name	Metal content[a] [%]		a_o [nm]	S_{BET}[b] [m²/g]	V_{total}[c] [cc/g]	P_D[d] [nm]	P_W[e] [nm]	Total acidity[f] [mmol/g]	Metal crystallite Size[g] [nm]	
	Ni	Ru							NiO	RuO$_2$
AlSBA15(25)[55*]	-	-	15.7	909	1.4	11.4	4.3	0.25	-	-
7% NiO	6.36	-	11.8	502	0.96	11.3	0.5	0.11	18.3	-
1%RuO$_2$	-	0.89	11.1	520	1.17	9.3	1.8	0.09	-	17.7
0.2%RuO$_2$/7%NiO	0.18	6.41	-	464	0.91	11.1	-	0.10	73.1	75.0
0.4%RuO$_2$/7%NiO	0.34	6.44	-	423	0.88	11	-	0.15	72.2	71.0
0.6%RuO$_2$/7%NiO	0.55	6.30	-	384	0.84	9.5	-	0.19	74.2	74.5
0.8%RuO$_2$/7%NiO	0.75	6.32	-	365	0.79	8.1	-	0.22	75.5	76.3
1.0%RuO$_2$/7%NiO	0.97	6.50	10.2	340	0.74	8.1	2.1	0.23	75.2	74.7

[*]Si/Al ratio from ICP-OES analysis

[a] Actual metal content from ICP-OES analysis

[b] BET Surface area calculated from the adsorption branch of the N$_2$ isotherm

[c] Total Pore volume calculated from the adsorption branch of N$_2$ isotherm.

[d] Average mesopore diameter calculated from the adsorption branch using the BJH method.

[e] Wall thickness of the samples estimated according to the expression:

$P_w = a_0 - P_D$ where $(a_0 = 2d_{100}/\sqrt{3})$

[f] Values obtained from NH$_3$-TPD results

[g] Crystallite size of metal oxides calculated from XRD (wide angle) analysis using Debey-Scherrer equation

Table 2.

Catalyst	Reactor	Reactant	WHSV (h^{-1})	Temp (^{o}C)	Pressure	HDO yield (%)	References
1.0%Ru/7.0 Ni	fixed bed	Anisole	4.1771	400	atm	8	This work
0.8%Ru/7.0 Ni	fixed bed	Anisole	4.1771	400	atm	6	This work
0.6%Ru/7.0 Ni	fixed bed	Anisole	4.1771	400	atm	5	This work
0.4%Ru/7.0 Ni	fixed bed	Anisole	4.1771	400	atm	6	This work
0.2%Ru/7.0 Ni	fixed bed	Anisole	4.1771	450	atm	5	This work
Ni/C	continuous flow	Anisole	20.4	310	3 bar	64	[5]
copper chromite	Parr	Anisole	–	275	50 bar	26	[21]
Ni$_2$ P/SiO$_2$	continuous flow	Anisole	10	300	15 bar	14	[22]
HY Zeolite	tubular	Anisole	0.42	400	1 atm	–	[23]
Ni/γ-Alumina	fixed bed	Anisole	2	300	50 bar	–	[24]

Fig. 1 (a)

Fig. 1(b)

Fig. 2 (a)

Fig. 2(b)

Fig. 3

1.0% RuO$_2$/AlSBA-15(25), 7.0% NiO/AlSBA-15(25), AlSBA-15(25)
1.0% RuO$_2$/7.0% NiO/AlSBA-15(25), 0.8% RuO$_2$/7.0% NiO/AlSBA-15(25)
0.6% RuO$_2$/7.0% NiO/AlSBA-15(25), 0.4% RuO$_2$/7.0% NiO/AlSBA-15(25)
0.2% RuO$_2$/7.0% NiO/AlSBA-15(25)

TCD Signal (a.u.)

Temperature (°C)
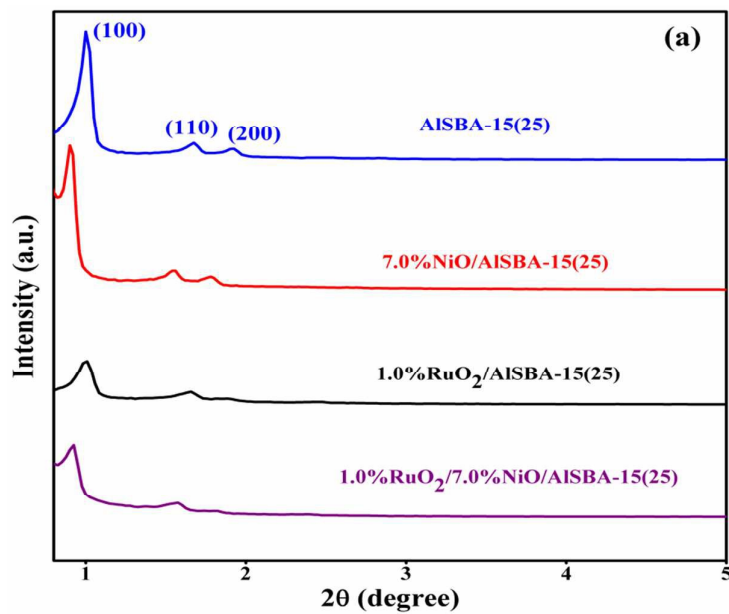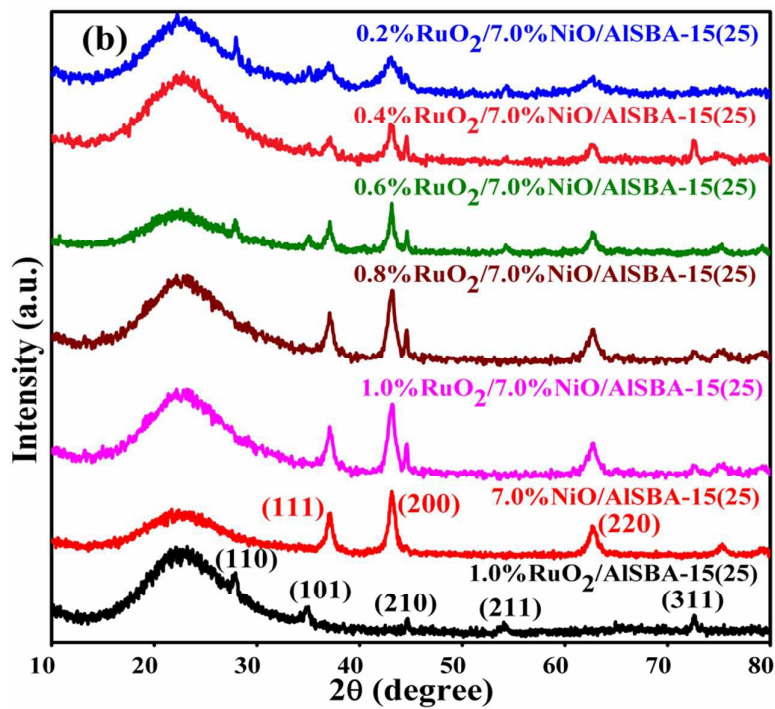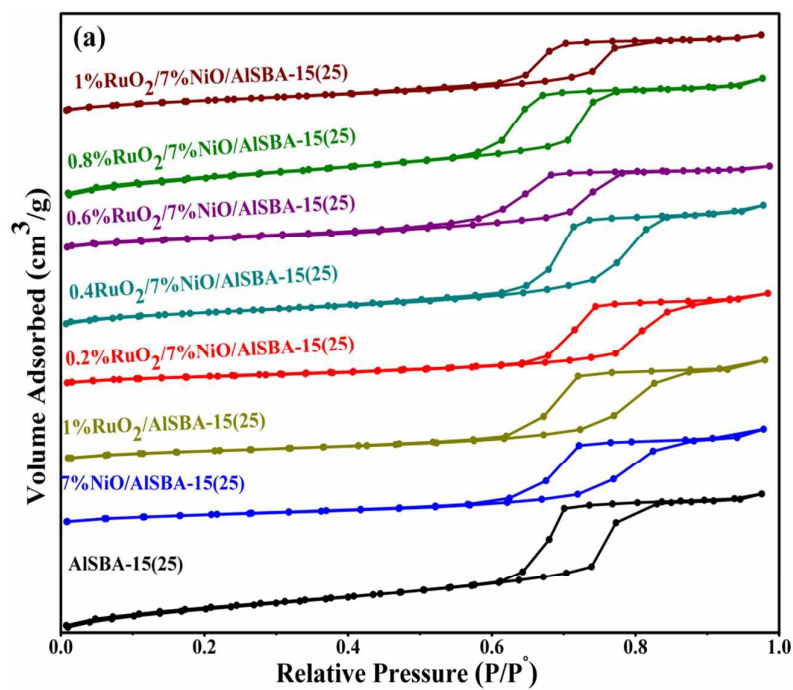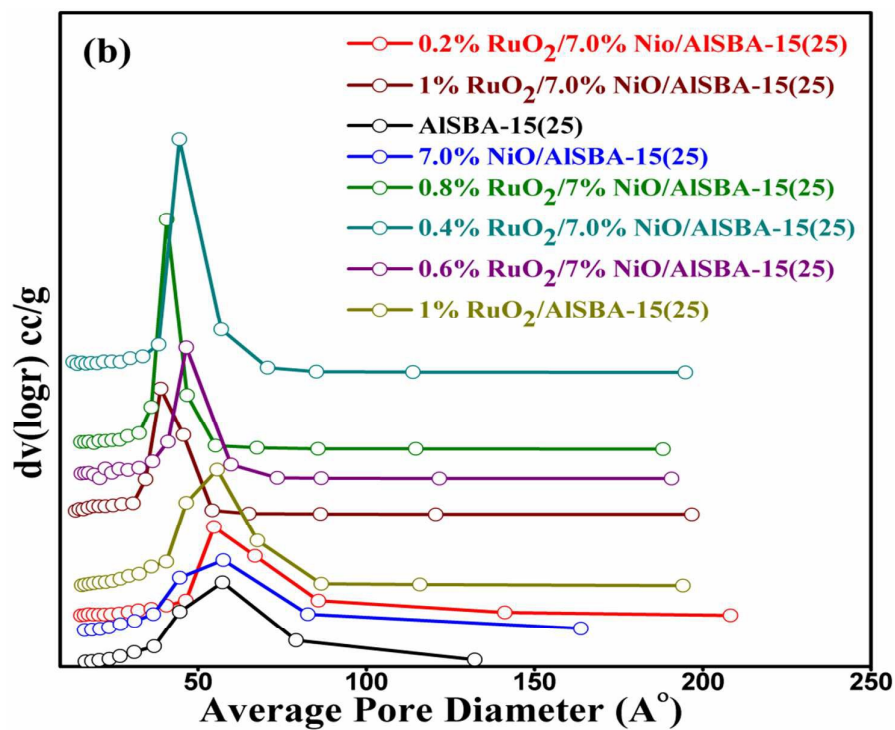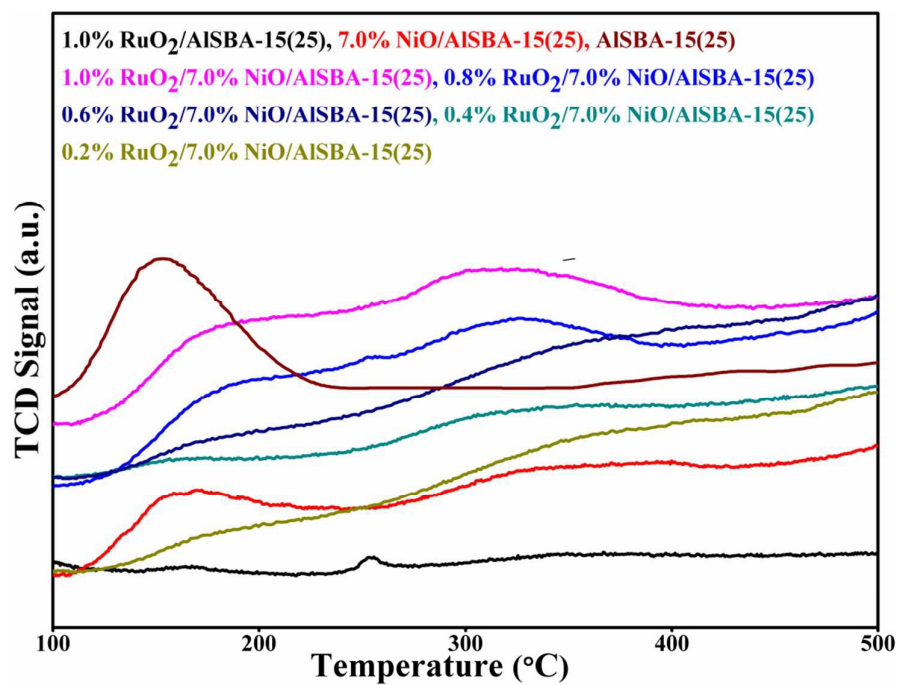
Fig. 4

Fig. 5

Fig. 6

Fig. 7

Fig, 8

Fig. 9

a) Demethylation
b) Methyltransfer
c) Hydrogenolysis
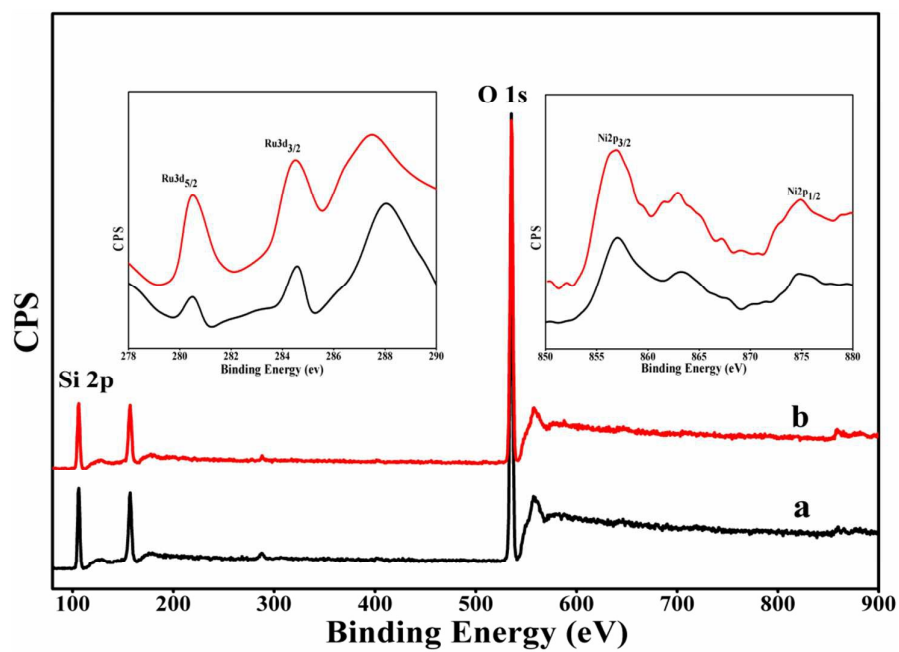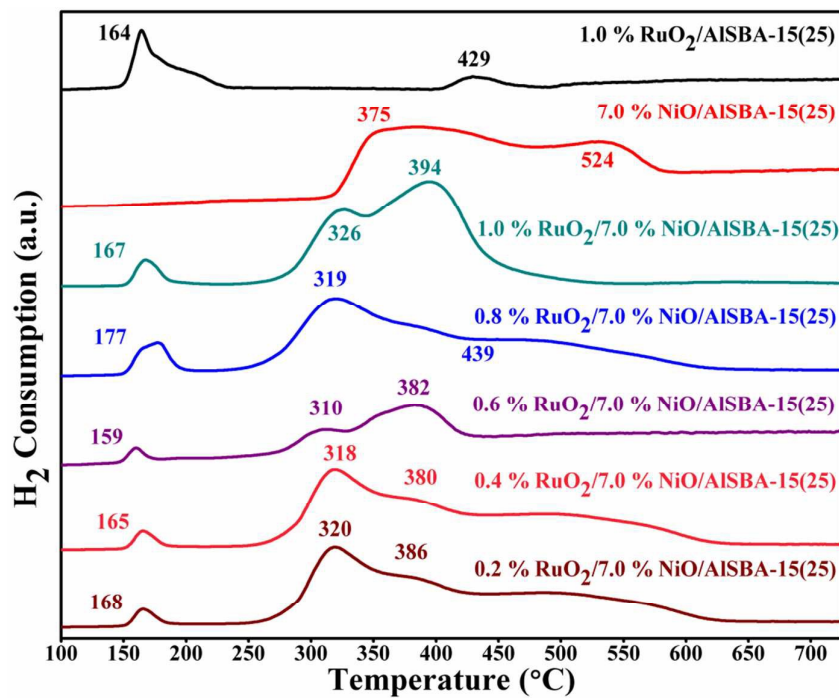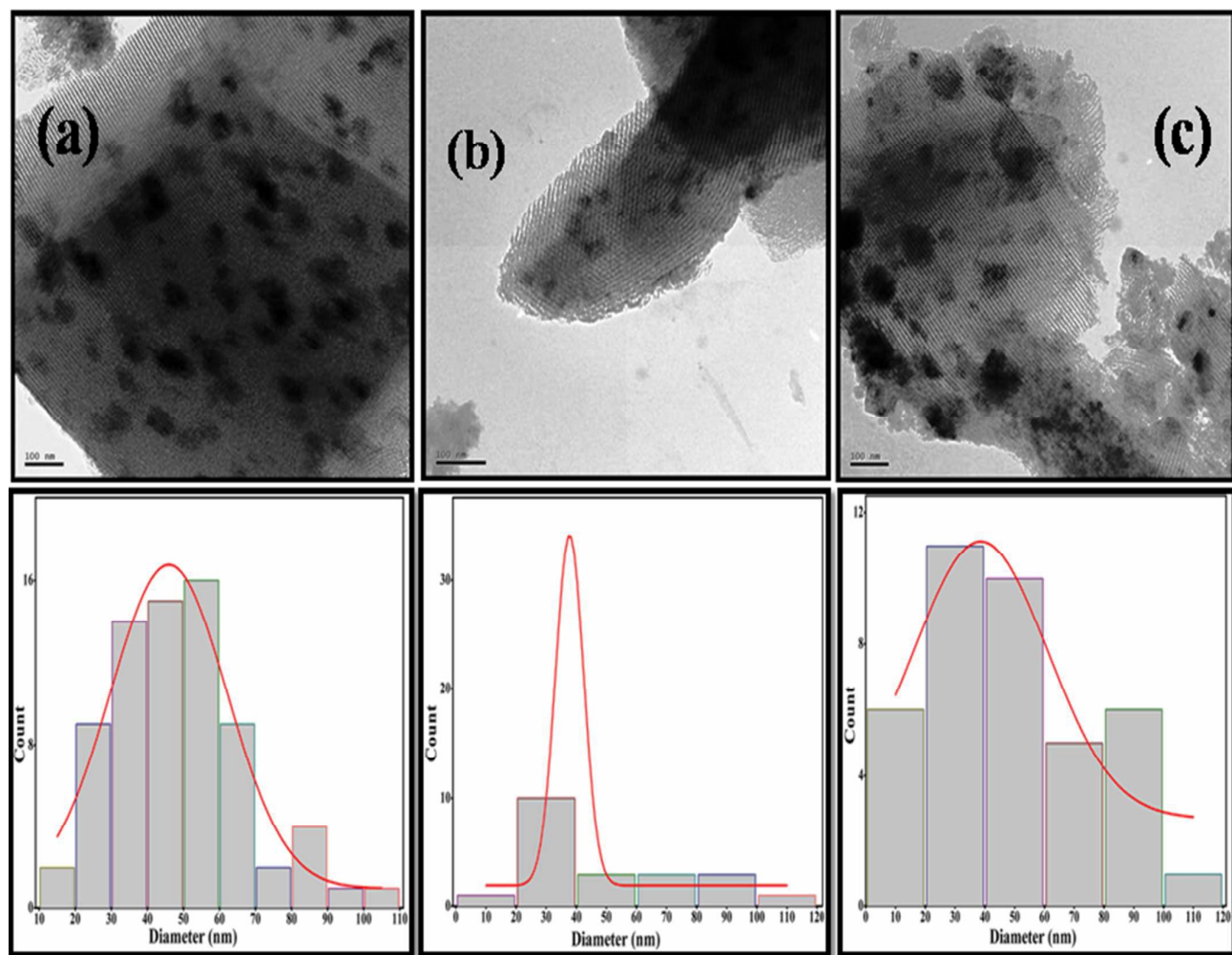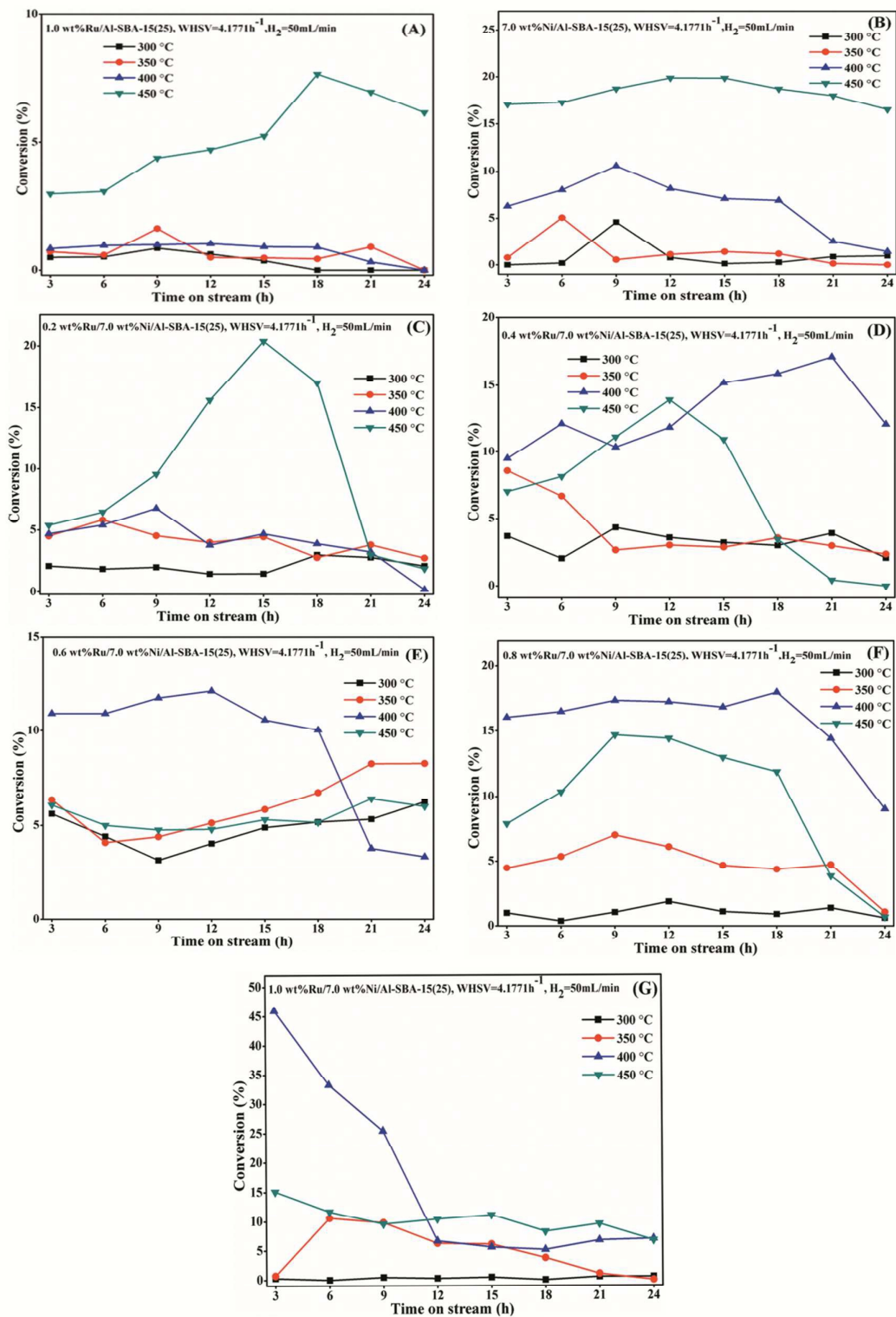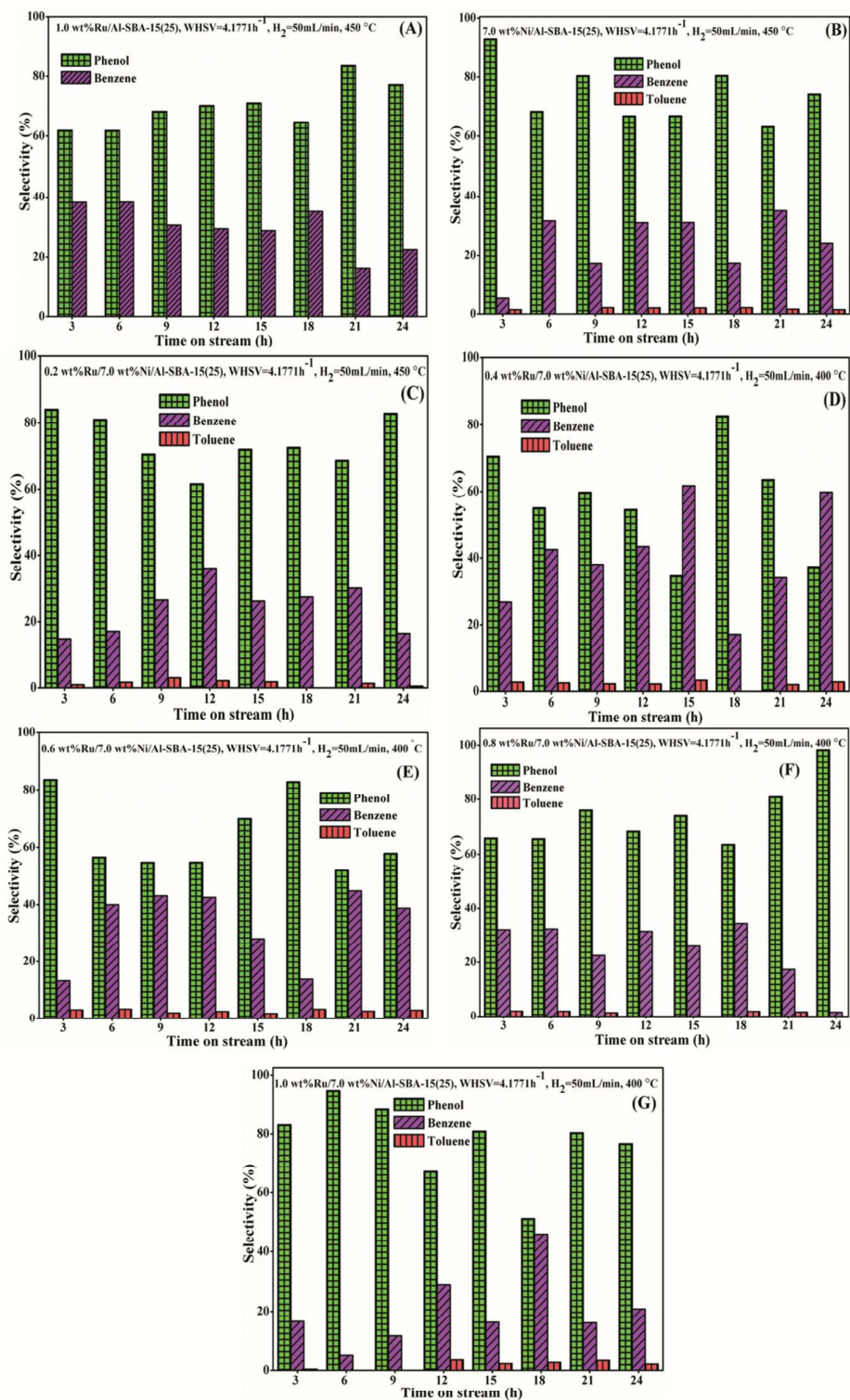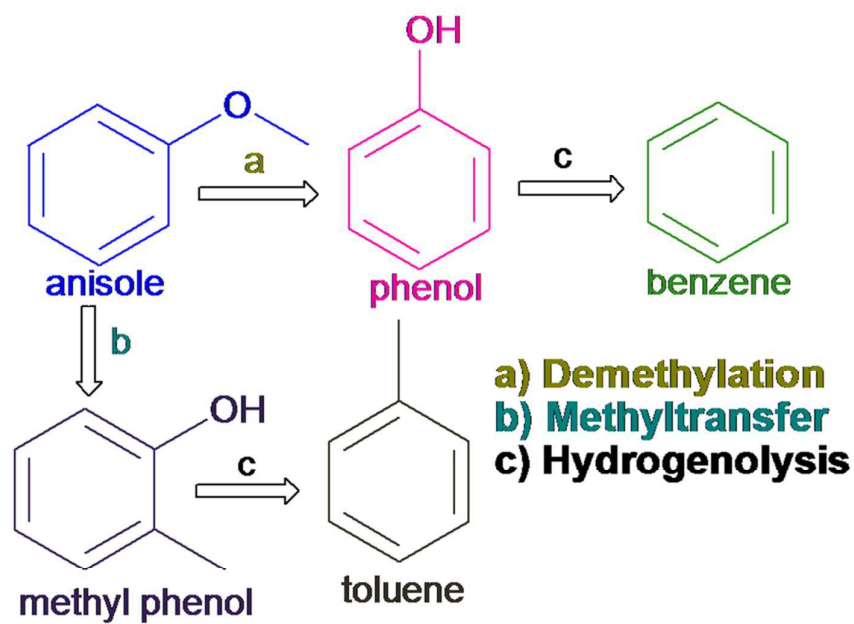
Fig. 10
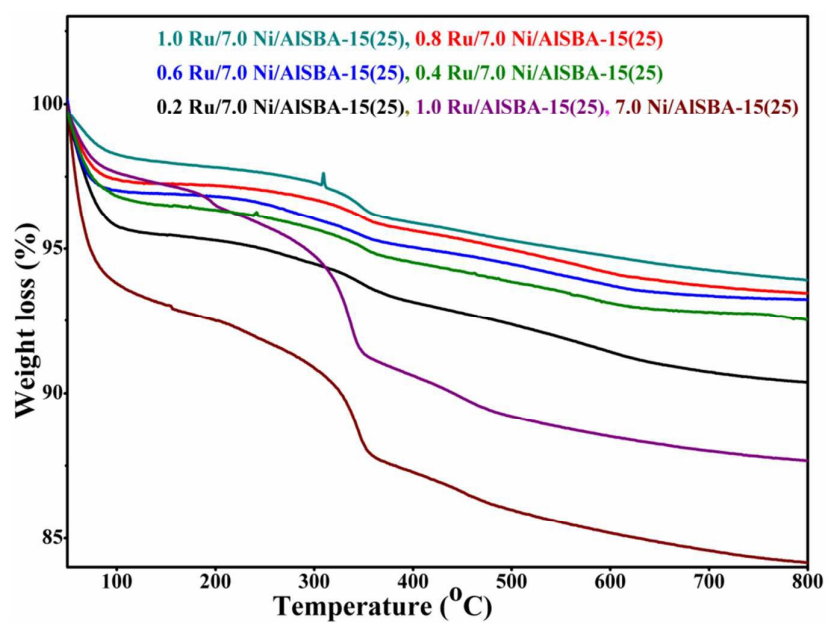
Fig. 11
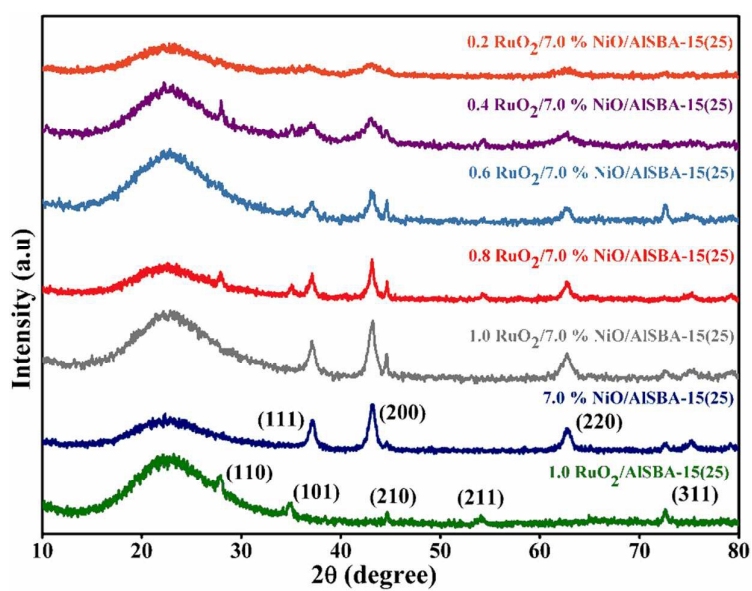
References

1   E. Furimsky, *Appl. Catal. A Gen.*, 2000, **199**, 147–190.

2   A. L. Jongerius, R. Jastrzebski, P. C. A. Bruijnincx and B. M. Weckhuysen, *J. Catal.*, 2012, **285**, 315–323.

3   A. Vinu, V. Murugesan, W. Böhlmann and M. Hartmann, *J. Phys. Chem. B*, 2004, **108**, 11496–11505.

4   S. K. Wu, P. C. Lai, Y. C. Lin, H. P. Wan, H. T. Lee and Y. H. Chang, *ACS Sustain. Chem. Eng.*, 2013, **1**, 349–358.

5   Y. Yang, C. Ochoa-Hernández, V. A. de la Peña O'Shea, P. Pizarro, J. M. Coronado and D. P. Serrano, *Appl. Catal. B Environ.*, 2014, **145**, 91–100.

6   S. Jin, Z. Xiao, C. Li, X. Chen, L. Wang, J. Xing, W. Li and C. Liang, *Catal. Today*, 2014, **234**, 125–132.

7   N. Yan, Yuan, R. Dykeman, Y. Kou and P. J. Dyson, *Angew. Chemie - Int. Ed.*, 2010, **49**, 5549–5553.

8   C. V. Loricera, B. Pawelec, A. Infantes-Molina, M. C. Álvarez-Galván, R. Huirache-Acuña, R. Nava and J. L. G. Fierro, *Catal. Today*, 2011, **172**, 103–110.

9   S. A. Khromova, A. A. Smirnov, O. A. Bulavchenko, A. A. Saraev, V. V Kaichev, S. I. Reshetnikov and V. A. Yakovlev, *"Applied Catal. A , Gen.*, 2014, **470**, 261–270.

10   W. Song, Y. Liu and E. Baráth, C. Zhao and J. A. Lercher, *Green Chem.*, 2014, **17**, 1204–1218.

11   K. V. R. Chary and C. S. Srikanth, *Catal. Letters*, 2009, **128**, 164–170.

12   A. Vinu, B. M. Devassy, S. B. Halligudi, W. Böhlmann and M. Hartmann, *Appl. Catal. A Gen.*, 2005, **281**, 207–213.

13   J. L. Liu, L. J. Zhu, Y. Pei, J. H. Zhuang, H. Li, H. X. Li, M. H. Qiao and K. N. Fan, *Appl. Catal. A , Gen.*, 2009, **353**, 282–287.

14   M. Lindo, A. J. Vizcaíno, J. A. Calles and A. Carrero, *Int. J. Hydrogen Energy*, 2010, **35**, 5895–5901.

15   V. Sundaramurthy, I. Eswaramoorthi, A. K. Dalai and J. Adjaye, *Microporous Mesoporous Mater.*, 2008, **111**, 560–568.

16   A. Korotcov, H. P. Hsu, Y. S. Huang, T. S. Tsai and K. K. Tiong, Crystal *Growth&Design.,* 2006, **6**, 2501–2506.

17   S. A. El-Safty, Y. Kiyozumi, T. Hanaoka and F. Mizukami, *Appl. Catal. A Gen.*, 2008, **337**, 121–129.

18   T. M. Sankaranarayanan, A. Berenguer, C. Ochoa-hernández, I. Moreno, P. Jana, J. M. Coronado, D. P. Serrano and P. Pizarro, *Catal. Today*, 2015, **243**, 163–172.

19   F. V. Barsi and D. Cardoso, *Brazilian J. Chem. Eng.*, 2009, **26**, 353–360.

20   C. Crisafulli, S. Scirè, S. Minicò and L. Solarino, *Appl. Catal.*, 2002, **225**, 1–9.

21   C. Wang, L. Zhang and Y. Liu, *Appl. Catal. B Environ.*, 2013, **136-137**, 48–55.

22   X. Zhu, L. L. Lobban, R. G. Mallinson and D. E. Resasco, *J. Catal.*, 2011, **281**, 21–29.

23   K. L. Deutsch and B. H. Shanks, *"Applied Catal. A, Gen.*, 2012, **447-448**, 144–150.

24   K. Li, R. Wang and J. Chen, *Energy & Fuels.*, 2011, **25**, 854–863.

25   T. Prasomsri, A. T. To, S. Crossley, W. E. Alvarez and D. E. Resasco, *"Applied Catal. B, Environ.*, 2011, **106**, 204–211.

26   M. Saidi, F. Samimi, D. Karimipourfard, T. Nimmanwudipong, B. C. Gates and M. R. Rahimpour, *Energy Environ. Sci.*, 2014, **7**, 103.

27   J. E. Peters, J. R. Carpenter and D. C. Dayton, *Energy & Fuels.*, 2015, **29**, 909-916.

28   V. A. Yakovlev, S. A. Khromova, O. V Sherstyuk, V. O. Dundich, D. Y. Ermakov, V. M. Novopashina, M. Y. Lebedev, O. Bulavchenko and V. N. Parmon, *Catal. Today.,* 2009, **144**, 362–366.

29   W. Lee, Z. Wang, R. J. Wu and A. Bhan, *J. Catal.*, 2014, **319**, 44–53.